Lawrence Berkeley National Laboratory

LBL Publications

Title

Controlling spin-orbit coupling strength of bulk transition metal dichalcogenide semiconductors

Permalink

https://escholarship.org/uc/item/4jc641m2

Authors

Lee, Yeonghoon

Eu, Pilsun

Lim, Chan-young

et al.

Publication Date

2021-10-01

DOI

10.1016/j.cap.2021.03.008

Copyright Information

This work is made available under the terms of a Creative Commons Attribution-NonCommercial License, available at https://creativecommons.org/licenses/by-nc/4.0/

Peer reviewed

eScholarship.org Powered by the California Digital Library
University of California

Controlling spin-orbit coupling strength of bulk transition metal dichalcogenide semiconductors

Yeonghoon Lee[1], Pilsun Eu[1], Chan-young Lim[1], Jaehun Cha[1], Sunghun Kim[1], Jonathan D. Denlinger[2], Yeongkwan Kim[1,*]

[1] Department of Physics, Korea Advanced Institute of Science and Technology, Daejeon 34141, Republic of Korea.

[2] Advanced Light Source, Lawrence Berkeley National Laboratory, Berkeley, California 94720, USA.

Abstract

Transition metal dichalcogenide (TMD) semiconductors are attracting much attention in research regarding device physics based on their unique properties that can be utilized in spintronics and valleytronics. Although current studies concentrate on the monolayer form due to the explicitly broken inversion symmetry and the direct band gap, bulk materials also hold the capability of carrying spin and valley current. In this study, we report the methodology to continuously control the spin-orbit coupling (SOC) strength of bulk TMDs $Mo_{1-x}W_xSe_2$ by changing the atomic ratio between Mo and W. The results show the size of band splitting at the K valley the measure of the coupling strength is linearly proportional to the atomic ratio of Mo and W. Our results thus demonstrate how to precisely tune the SOC coupling strength, and the collected information of which can serve as a reference for future applications of bulk TMDs.

Keywords

Transition metal dichalcogenide semiconductor, spintronics, valleytronics, spin-orbit coupling, angle-resolved photoemission spectroscopy

1. Introduction

Two-dimensional transition metal dichalcogenide (TMD) semiconductors 2H-MX_2 (M = Mo, W; X = S, Se, Te) have attracted much attention due to the possibilities of applications in spintronic and valleytronic devices [1–8]. By virtue of the lattice symmetry with explicitly broken inversion symmetry, spin-dependent, valley-dependent, and Berry curvature dependent properties are expected. Up to now, most of the research has focused on the monolayer system, whereas bulk 2H-MX_2 has attracted relatively less interest due to two major disadvantages. First, the restored inversion symmetry in the bulk form causes spin degeneracy, which hinders the formation of a spin current or other properties associated with the Berry curvature. In the atomic and electronic structure of bulk 2H-MX_2 (Figs. 1(a) and (b)), the inversion symmetry generates nearly degenerate bands at the K valleys as spin-split

bands when the spin-orbit coupling (SOC) of the two layers are oppositely combined (Fig. 1(c)). Second, the valence band maximum (VBM) and the conduction band minimum (CBM) of the monolayer is located at the K valleys and form a direct band gap, whereas those of the bulk result in an indirect band gap [9–13]. This direct-to-indirect band gap transition from monolayer to bulk renders the use of bulk MX_2 unfavorable for the optoelectric devices and field-effect transistors.

However, recent studies have revealed that bulk MX_2 can be used for spintronic and valleytronic devices. In the case of WSe_2, the bulk band is spin-polarized even with the inversion symmetry [14] and it is possible to induce the indirect-to-direct bandgap transition by applying strain to the multilayer system [15]. Additionally, surface doping of alkali metals on TMD semiconductors produces spin-splitting by breaking the inversion symmetry, which changes the CBM to the K point as well as the VBM to the K point to form a direct band gap in the case of $MoTe_2$ [16, 17]. Furthermore, it is demonstrated that even in the absence of a direct bandgap, bulk TMD semiconductors can also produce valley and spin currents by employing a circularly polarized light source [18].

Despite the growing possibilities of utilizing bulk TMD semiconductors, only a few attempts have been made to tune the SOC of the bulk, which directly influences the band gap of the bulk TMD as well as its spin- and valley-dependent responses. In this work, we report the results of successfully controlled SOC of a TMD semiconductor by exchanging the transition metals. By analyzing $Mo_{1-x}W_xSe_2$ single crystals using energy-dispersive X-ray spectroscopy (EDS) and angle-resolved photoemission spectroscopy (ARPES), we demonstrate that the band splitting at the K points is linearly proportional to the W composition ratio. The results not only illustrate the methodology to control SOC in TMD semiconductors but can also serve as a reference for the future applications of bulk TMD in both valleytronics and spintronics.

2. Methods

$Mo_{1-x}W_xSe_2$ single crystals were grown by the chemical vapor transport (CVT) method. In addition to the stoichiometric amounts of tungsten (purity: 99.99%), molybdenum (purity: 99.99%), and selenium (purity: 99.999%) powder, more selenium or iodine (purity: 99.999%) was added as a transport agent. The mixed powders were put into quartz ampoules, sealed in high-vacuum conditions (~10^{-5} torr), and then transferred to a two-zone furnace. After the crystals were removed from the ampoules, EDS measurements were conducted for selected crystals after cleavage using the Magellan 400, scanning Electron Microscope at The Analysis Center for Research Advancement in the Korea Advanced Institute of Science and Technology. The details of the CVT conditions and the atomic ratio of Mo and W obtained from the EDS measurements are listed in Table 1.

The very same crystals were then transferred ex situ to beamline 4.0.3 at the Advanced Light Source

(ALS) to perform angle-resolved photoemission spectroscopy (ARPES). Samples were cleaved in situ at 60 K for WSe_2 and at 80 K under ultra-high vacuum better than 10^{-10} torr. The incident photon energy was fixed at 70 eV; however, the photon energy has little effect on the band splitting size at the K valleys [19]. The total energy resolution was 25 meV for WSe_2 and 34 meV, estimated with the reference gold spectrum. A Scienta R8000 electron spectrometer was used to collect the electrons.

3. Results and discussion

The scanning electron microscope (SEM) images and the corresponding EDS spectra of samples 2, 3, and 6 in Table 1 are presented in Figure 2. The crystals have a hexagonal structure as expected from the atomic structure with a flat surface. The dimensions of the crystals varied from 0.5 * 0.5 mm^2 to 1.5 * 1.5 mm^2. The change in the Mo and W peaks was observed from the EDS spectra (Fig. 2(b)) and the integrations of the peak intensities were used to estimate the actual mole ratio of each crystal summarized in Table 1. The full doping range from 0 to 1 was explored with a sufficient number of doping levels.

Fig. 3(a) shows the band dispersions along the Γ-K direction of $Mo_{1-x}W_xSe_2$ with different doping levels. For all doping levels, the VBMs were located at the Γ point, which is characteristic of the bulk. The bands split into two nearly spin-degenerate bands upon dispersing toward the K point. It can be observed that the size of splitting gradually increases as the W doping level increases. To accurately measure the band splitting at each level, an energy distribution curve (EDC) fitting was performed for the EDC at the K points (Fig. 2(b)), determining the peak positions in the binding energy. The fitted results illustrate that the splitting gradually increases from 210 meV to 478 meV as the doping level increases, in which the two end values correspond well to the previous study [19].

Combined with the EDS results for each sample, the relationship between the band splitting and the W composition is plotted in Figure 4. The results show that the band splitting and the W composition are linearly proportional. In the case of monolayer $Mo_{1-x}W_xSe_2$, density functional theory (DFT) calculations have already predicted this linear proportionality [6]. Although it is known that band splitting is expected in the bulk case even without SOC [12, 20] through the interlayer interaction, such effect does not seem to affect the linear increase in the valence band splitting. The R-squared value of the fitted line (dashed line in Fig. 4) is 0.997, indicating that SOC is the key parameter in the splitting and can be tuned precisely by transition metal exchange.

Note that up to the highest doping rate of 0.884 (sample 8 in Table 1), the band splitting strictly follows a linear proportionality. Because there is only a small amount of Mo atoms in the crystal, it is highly likely that the Mo atom is non-uniformly and discretely distributed. This could result in a

variation in the splitting size at different locations, producing multiple sets of splitting bands in the measurements from the combination of information at different locations. However, the occurrence of one set of splitting bands in all data sets indicates the uniform SOC strength at least within the area where the collected photoelectrons were excited by the photon beam, which is typically on the scale of several tens of micrometers. This implies that although the nature of SOC is local, the effects of combining the elements with distinct SOC strength can be spread non-locally, at least for the doping levels evaluated in the present study.

4. Conclusion

In conclusion, we have synthesized $Mo_{1-x}W_xSe_2$ covering the full doping range and successfully controlled the SOC. We have observed band splitting at the K valley, demonstrating that SOC strength linearly increases when replacing Mo atoms with W atoms. The results show that the valence band splitting of bulk $Mo_{1-x}W_xSe_2$ conforms to the calculations for the monolayer TMD. To obtain full band gap information, further research on the bulk conduction band, which is known to spin-split in the monolayer limit, is needed. Nevertheless, the comprehensive information on specific SOC strength in certain doping level provided by the present work can lay the foundation for future applications of bulk TMD devices.

Declaration of competing interest

The authors declare that they have no known competing financial interests or personal relationships that could have appeared to influence the work reported in this paper.

Acknowledgments

This research used the resources at the Advanced Light Source, a U.S. DOE Office of Science User Facility under contract no. DE-AC02-05CH11231. This research was supported by the National R&D Program (No.2018K1A3A7A09056310), Creative Materials Discovery Program (No.2015M3D1A1070672), and Basic Science Resource Program (No.2017R1A4A1015426, No.2018R1D1A1B07050869) through the National Research Foundation of Korea (NRF) funded by the Ministry of Science, ICT and Future Planning and by the Internal R&D Program at KAERI funded by the Ministry of Science and ICT (MSIT) of the Republic of Korea (525350-19).

References

[1] T. Cao, G. Wang, W. Han, H. Ye, C. Zhu, J. Shi, Q. Niu, P. Tan, E. Wang, B. Liu, J. Feng, Valley-selective circular dichroism of molybdenum disulphide, Nat. Commun. 3 (2012) 887. https://doi.org/10.1038/ncomms1882.

[2] H. Zeng, J. Dai, W. Yao, D. Xiao, X. Cui, Valley polarization in MoS_2 monolayers by optical pumping,

Nat. Nanotech. 7 (2012) 490-493. https://doi.org/10.1038/nnano.2012.95.

[3] K. F. Mak, K. He, J. Shan, T. F. Heinz, Control of valley polarization in monolayer MoS_2 by optical helicity, Nat. Nanotech. 10 (2012) 494-498. https://doi.org/10.1038/nnano.2012.96.

[4] X. Xu, W. Yao, D. Xiao, T. F. Heinz, Spin and pseudospins in layered transition metal dichalcogenides, Nat. Phys. 10 (2014) 343-350. https://doi.org/10.1038/nphys2942.

[5] M. Zhang, J. Wu, Y. Zhu, D. O. Dumcenco, J. Hong, N. Mao, S. Deng, Y. Cehn, Y. Yang, C. Jin, S. H. Chaki, Y.-S. Huang, J. Zhang, L. Xie, Two-dimensional molybdenum tungsten diselenide alloys: photoluminescence, Raman scattering, and electrical transport, ACS Nano 8 (7) (2014) 7130-7137. https://doi.org/10.1021/nn5020566.

[6] G. Wang, C. Robert, A. Suslu, B. Chen, S. Yang, S. Alamdari, I. C. Gerber, T. Amand, X. Marie, S. Tongay, B. Urbaszek, Spin-orbit engineering in transition metal dichalcogenide alloy monolayers, Nat. Commun. 6 (2015) 10110. https://doi.org/10.1038/ncomms10110.

[7] Y. K. Luo, J. Xu, T. Zhu, G. Wu, E. J. McCormick, W. Zhan, M. R. Neupane, R. K. Kawakami, Opto-valleytronic spin injection on monolayer MoS_2/few-layer graphene hybrid spin valves, Nano Lett. 17 (6) (2017) 3877-3883. https://doi.org/10.1021/acs.nanolett.7b01393.

[8] S. Manzeli, D. Ovchinnikov, D. Pasquier, O. V. Yazyev, A. Kis, 2D transition metal dichalcogenides, Nat. Rev. Mater. 2 (2017) 17033. https://doi.org/10.1038/natrevmats.2017.33

[9] Z. Y. Zhu, Y. C. Cheng, U. Schwingenschlögl, Giant spin-orbit-induced spin splitting in two-dimensional transition-metal dichalcogenide semiconductors, Phys. Rev. B 84 (2011) 153402. https://doi.org/10.1103/PhysRevB.84.153402.

[10] W. S. Yun, S. W. Han, S. C. Hong, I. G. Kim, J. D. Lee, Thickness and strain effects on electronic structures of transition metal dichalcogenides: 2H-MX2 semiconductors (M=Mo, W; X=S, Se, Te), Phys. Rev. B 85 (2012) 033305. https://doi.org/10.1103/PhysRevB.85.033305.

[11] Y. Zhang, T.-R. Chang, B. Zhou, Y.-T. Cui, H. Yan, Z. Liu, F. Schmitt, J. Lee, R. Moore, Y. Chen, H. Lin, H.-T. Jeng, S.-K. Mo, Z. Hussain, A. Bansil, Z.-X. Shen, Direct observation of the transition from indirect to direct bandgap in atomically thin epitaxial $MoSe_2$, Nat. Nanotech. 9 (2014) 111-115. https://doi.org/10.1038/nnano.2013.277.

[12] N. Alidoust, G. Bian, S.-Y. Xu, R. Sankar, M. Neupane, C. Liu, I. Belopolski, D.-X. Qu, J. D. Denlinger, F.-C. Chou, M. Z. Hasan, Observation of monolayer valence band spin-orbit effect and induced quantum well states in MoX2, Nat. Commun. 5 (2014) 4673. https://doi.org/10.1038/ncomms5673.

[13] Y. Zhang, M. M. Ugeda, C. Jin, S.-F. Shi, A. J. Bradley, A. Martín-Recio, H. Ryu, J. Kim, S. Tang, Y. Kim, B. Zhou, C. Whang, Y. Chen, F. Wang, M. F. Crommie, Z. Hussain, Z.-X. Shen, S.-K. Mo, Electronic

structure, surface doping, and optical response in epitaxial WSe_2 thin films, Nano Lett. 16 (4) (2016) 2485-2491. https://doi.org/10.1021/acs.nanolett.6b00059.

[14] J. M. Riley, F. Mazzola, M. Dendzik, M. Michiardi, T. Takayama, L. Bawden, C. Granerød, M. Leandersson, T. Balasubramanian, M. Hoesch, T. K. Kim, H. Takagi, W. Meevasana, Ph. Hofmann, M. S. Bahramy, J. W. Wells, P. D. C. King, Direct observation of spin-polarized bulk bands in an inversion-symmetric semiconductor, Nat. Phys. 10 (2014) 835-839. https://doi.org/10.1038/nphys3105.

[15] S. B. Desai, G. Seol, J. S. Kang, H. Fang, C. Battaglia, R. Kapadia, J. W. Ager, J. Guo, A. Javey, Strain-induced indirect to direct bandgap transition in multilayer WSe_2, Nano Lett. 14 (8) (2014) 4592-4597. https://doi.org/10.1021/nl501638a.

[16] J. M. Riley, W. Meevasana, L. Bawden, M. Asakawa, T. Takayama, T. Eknapakul, T. K. Kim, M. Hoesch, S.-K. Mo, H. Takagi, T. Sasagawa, M. S. Bahramy, P. D. C. King, Negative electronic compressibility and tunable spin splitting in WSe_2, Nat. Nanotech. 10 (2015) 1043-1047. https://doi.org/10.1038/nnano.2015.217.

[17] M. Kang, B. Kim, S. H. Ryu, S. W. Jung, J. Kim, L. Moreschini, C. Jozwiak, E. Rotenberg, A. Bostwick, K. S. Kim, Universal mechanism of band-gap engineering in transition-metal dichalcogenides, Nano Lett. 17 (3) (2017) 1610-1615. https://doi.org/10.1021/acs.nanolett.6b04775.

[18] H. Yuan, X. Wang, B. Lian, H. Zhang, X. Fang, B. Shen, G. Xu, Y. Xu, S.-C. Zhang, H. Y. Hwang, Y. Cui, Generation and electric control of spin-valley coupled circular photogalvanic current in WSe_2, Nat. Nanotech. 9 (2014) 851-857. https://doi.org/10.1038/nnano.2014.183.

[19] B. S. Kim, J.-W. Rhim, B. Kim, C. Kim, S. R. Park, Determination of the band parameters of bulk 2H-MX_2 (M=Mo, W; X=S, Se) by angle-resolved photoemission spectroscopy, Sci. Rep. 6 (2016) 36389. https://doi.org/10.1038/srep36389.

[20] Y.-H. Zhao, F. Yang, J. Wang, H. Guo, W. Ji, Continuously tunable electronic structure of transition metal dichalcogenides superlattices, Sci. Rep. 5 (2015) 8356. https://doi.org/10.1038/srep08356.

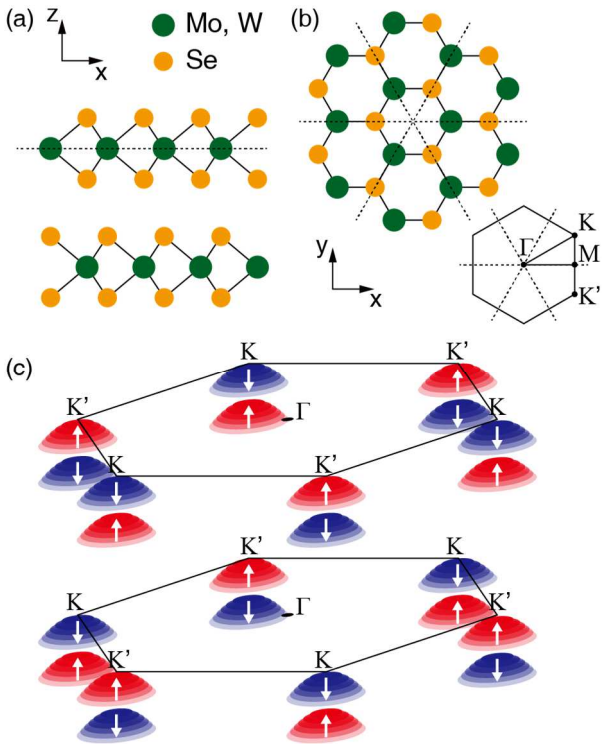

Fig. 1. (a) Side view and (b) top view of the crystal structure of 2H-MX_2. The dashed lines are mirror planes. The inset in (b) represents the Brillouin zone of 2H-MX_2. (c) Schematics of K and K′ valleys. The lack of inversion symmetry for the monolayer causes spin-splitting, whereas in the bulk case, the bands are nearly spin-degenerate due to the symmetry.

Table 1. Details of the CVT growth conditions and the EDS results of $Mo_{1-x}W_xSe_2$ crystals.

	Initial material		Ampoule dimension		Temperature distribution			EDS results
Sample	Mole ratio (Mo : W)	Transport agent	Length (mm)	Diameter (mm)	Hot zone (℃)	Cold zone (℃)	Growth time (h)	W ratio
1	1 : 0	Se	170	25	880	810	456	0
2	9 : 1	Se	170	25	910	850	456	0.278
3	5 : 5	I_2	160	25	890	810	288	0.464
4	7 : 3	Se	170	25	880	810	720	0.513
5	8 : 2	Se	170	25	880	810	720	0.528
6*	3 : 7	Se	170	25	880	810	720	0.784
7*								0.816
8	4 : 6	Se	170	25	880	810	720	0.884
9	0 : 1	Se	170	25	880	810	456	1

*Samples 6 and 7 are removed from the same ampoule.

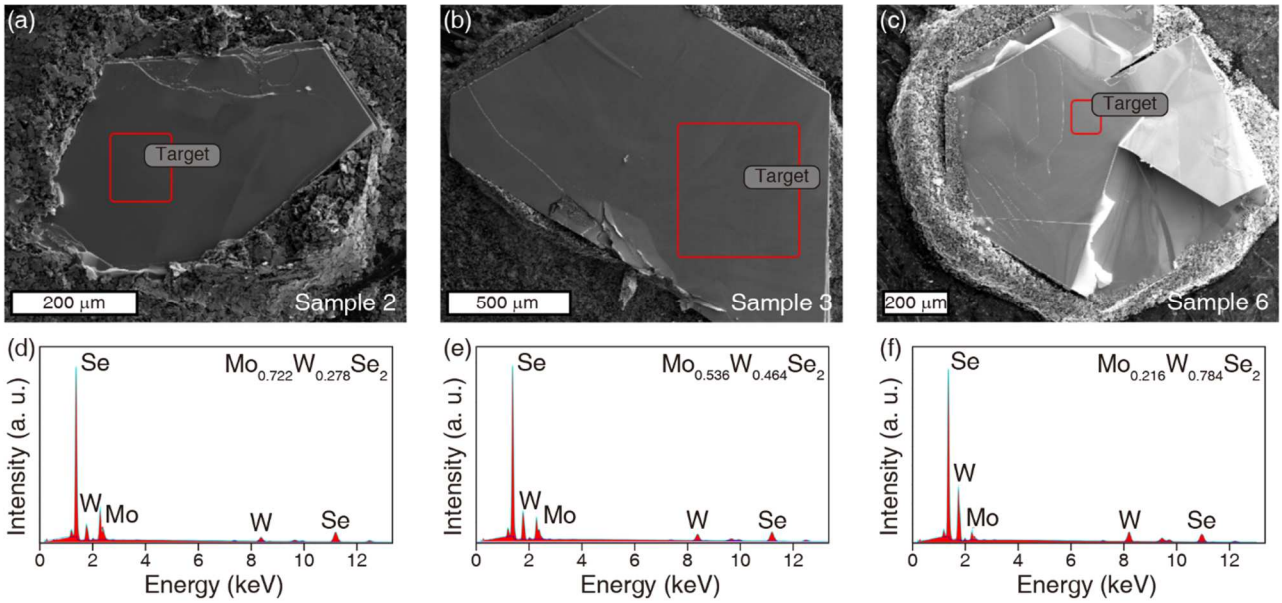

Fig. 2. (a–c) SEM image of samples 2 (a), 3 (b), and 6 (c) listed in Table 1. (d–f) The EDS spectra of samples 2 (d), 3 (e), and 6 (f) of the area inside the red box of Figs. (a–c).

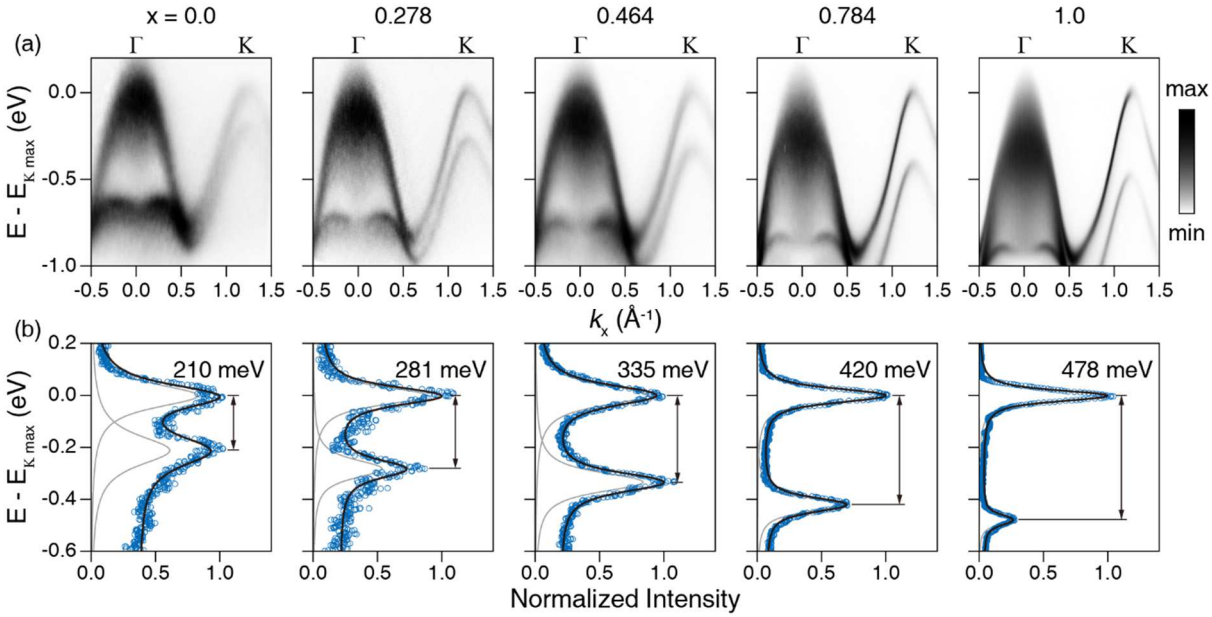

Fig. 3. (a) Band dispersions of the selected $Mo_{1-x}W_xSe_2$ (samples 1, 2, 3, 6, and 9 listed in Table 1) measured by ARPES. (b) EDC spectra at the K point for each doping level with a fitted curve. The dark blue circles are the normalized intensity, whereas the black and gray solid curves are the results of fitting using the Lorentzian functions convolved with Gaussian curve, accounting for the experimental resolution.

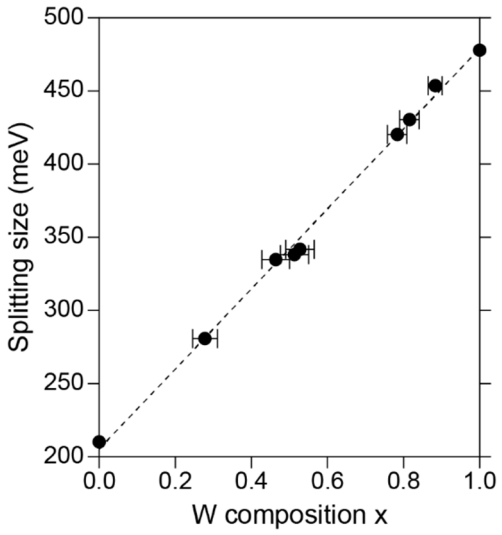

Fig. 4. Band splitting size in terms of W composition. The dashed line is the fitted line where the splitting size is calculated as 205.34 + 273.59x meV with an R-squared value of 0.997. The error bar along the energy direction is smaller than the marker size for every data point.